University Library



A gateway to Melbourne's research publications

Minerva Access is the Institutional Repository of The University of Melbourne

Author/s:
Alquethamy, S;Ganio, K;Luo, Z;Hossain, SI;Hayes, AJ;Ve, T;Davies, MR;Deplazes, E;Kobe, B;McDevitt, CA

Title:
Structural and biochemical characterization of Acinetobacter baumannii ZnuA

Date:
2022-06-01

Citation:
Alquethamy, S., Ganio, K., Luo, Z., Hossain, S. I., Hayes, A. J., Ve, T., Davies, M. R., Deplazes, E., Kobe, B. & McDevitt, C. A. (2022). Structural and biochemical characterization of Acinetobacter baumannii ZnuA. Journal of Inorganic Biochemistry, 231, https://doi.org/10.1016/j.jinorgbio.2022.111787.

Persistent Link:
https://hdl.handle.net/11343/300002

Revised Manuscript Clean version Click here to view linked References

Structural and biochemical characterization of *Acinetobacter baumannii* ZnuA

Saleh Alquethamy[1], Katherine Ganio[1], Zhenyao Luo[2,3,4], Sheik Imamul Hossain[5], Andrew J. Hayes[1], Thomas Ve[2,3,4,6], Mark R. Davies[1], Evelyne Deplazes[2,5], Boštjan Kobe[2,3,4,†], Christopher A. McDevitt[1,†]

1. Department of Microbiology and Immunology, The Peter Doherty Institute for Infection and Immunity, The University of Melbourne, Melbourne, Victoria, Australia.
2. School of Chemistry and Molecular Biosciences, The University of Queensland, Brisbane, Queensland, Australia.
3. Australian Infectious Diseases Research Centre, The University of Queensland, Brisbane, Queensland, Australia.
4. Institute for Molecular Bioscience, The University of Queensland, Brisbane, Queensland, Australia.
5. School of Life Sciences, University of Technology Sydney, Ultimo, New South Wales, Australia.
6. Present Address: Institute for Glycomics, Griffith University, Queensland, Australia.

† Correspondence address: Boštjan Kobe, School of Chemistry and Molecular Biosciences, The University of Queensland, Brisbane, Queensland, Australia. Phone: +61-7-3365-2132. E-mail: b.kobe@uq.edu.au; Christopher A. McDevitt, Department of Microbiology and Immunology, The Peter Doherty Institute for Infection and Immunity, The University of Melbourne, Melbourne, Victoria, 3000, Australia. Phone: 61-3-8344-7200. E-mail: christopher.mcdevitt@unimelb.edu.au;

Keywords: *Acinetobacter baumannii*, zinc, solute-binding protein, ABC transporter, ZnuA, zinc homeostasis

Running title: Characterization of *A. baumannii* ZnuA

ABSTRACT

Acinetobacter baumannii is a Gram-negative nosocomial pathogen associated with significant disease. Crucial to the survival and pathogenesis of *A. baumannii* is the ability to acquire essential micronutrients such as Zn(II). Recruitment of Zn(II) by *A. baumannii* is mediated, at least in part, by the periplasmic solute-binding protein ZnuA and the ATP-binding cassette transporter ZnuBC. Here, we combined genomic, biochemical, and structural approaches to characterize *A. baumannii* AB5075_UW ZnuA. Bioinformatic analyses using a diverse collection of *A. baumannii* genomes determined that ZnuA is highly conserved, with the binding site comprised by three strictly conserved histidine residues. The structure of metal-free ZnuA was determined at 2.1 Å resolution, with molecular dynamics revealing that loop α2β2, which harbors the putative Zn(II)-coordinating residue His41, was highly mobile in the metal-free state. The contribution of the putative binding site histidine residues to Zn(II) binding was further probed by mutagenesis. Analysis of ZnuA mutant variants was performed by quantitative metal binding assays, differential scanning fluorimetry and affinity measurements, which showed that all three histidine residues contributed to Zn(II)-recruitment, albeit to different extents. Collectively, these analyses provide insight into the mechanism of Zn(II)-binding by *A. baumannii* ZnuA and expand our understanding of the functional diversity of Zn(II)-recruiting proteins.

1. INTRODUCTION

The *d*-block metal ion zinc [Zn(II)] is the second most abundant transition metal ion in humans and is crucial for all life forms. Zinc is predicted to interact with approximately 6% of the proteome of prokaryotes, wherein the metal ion serves in structural and catalytic roles [1-3]. The essentiality of Zn(II) necessitates that pathogenic microorganisms use efficacious recruitment mechanisms to acquire the metal ion from the host environment. Accordingly, vertebrate hosts employ a variety of withholding mechanisms to restrict the bioavailability of nutrient metal ions such as Zn(II). To overcome Zn(II) withholding at the host-pathogen interface, bacteria such as *Acinetobacter baumannii* [4], *Pseudomonas aeruginos*a [5, 6], *Escherichia coli* [7], *Salmonella enterica* serovar Typhimurium [8], and *Streptococcus pneumoniae* [9-11] can employ a variety of high affinity Zn(II) scavenging mechanisms.

A. baumannii is an opportunistic human pathogen found predominantly in hospitals and aged-care facilities. The emergence of multidrug-resistant *A. baumannii* isolates has prompted the World Health Organization (WHO) and the Centers for Disease Control and Prevention (CDC) to classify *A. baumannii* as a serious threat to human health [12]. Acquisition of Zn(II) is essential for *A. baumannii* pathogenesis and survival, and its uptake is mediated by the ATP-binding cassette (ABC) transporter, ZnuBC, and the periplasmic solute-binding protein (SBP), ZnuA [4, 13]. Disruption of any component of the *A. baumannii* ZnuABC permease has been shown to result in a pronounced growth defect in Zn(II)-limited media and a lower bacterial burden in sepsis and pneumonia models of infection [4]. In addition to the ZnuABC permease, an outer membrane receptor, ZnuD1, and a Zn(II) metallochaperone, ZigA, have been shown to be necessary for *A. baumannii* survival in Zn(II) restricted conditions and infection in mice [4, 14]. Regulation of the Zn(II) acquisition machinery in *A. baumannii* is mediated by the Zn(II)-uptake regulator Zur, which belongs to the ferric uptake regulator (Fur) family of metalloregulators [15]. Zur mediates Zn(II)-dependent repression of the *znuABC*, *zigA*, and the *znuD1* pathways and thereby tightly regulates cellular abundance of Zn(II), in concert with metal ion-specific efflux pathways [16-18].

Here, we report the genomic, structural, and biochemical characterization of *A. baumannii* ZnuA. Amino acid sequence analyses indicated that the protein belongs to the Cluster A-I subgroup of SBPs associated with metal-specific prokaryotic ABC importers [19]. The structure of metal-free *A. baumannii* ZnuA revealed a canonical cluster A-I SBP fold, with molecular dynamics simulations predicting that loop α2β2, which contains the metal-coordinating residue histidine (His) 41, to be highly mobile in the absence of Zn(II). By contrast, the other metal-coordinating His residues appear to comprise a relatively static preformed metal-binding site. Analysis of ZnuA mutant variants revealed the relative contribution of the histidine residues in SBP interaction and affinity for Zn(II). Collectively, these analyses provide the basis to propose a potential mechanism for Zn(II)-binding by *A. baumannii* ZnuA, which further expands our knowledge of the conformational landscape sampled by cluster A-I SBPs.

2. MATERIALS AND METHODS

2.1 *A. baumannii* ZnuA sequence conservation within a global genomic framework

A global diversity framework of 292 publicly available *A. baumannii* genome assemblies were derived from The PATRIC Bioinformatics Resource Center [20]. Sequence conservation and prevalence of *A. baumannii* AB5075_UW (GenBank accession number: CP008706.1) gene products; ZnuA (ABUW_3740), ZnuB (ABUW_3743), ZnuC (ABUW_3742), ZnuD1 (ABUW_0600), ZigA (ABUW_0073), ZuR (ABUW_3741), GltA (ABUW_0867), GyrB (ABUW_0004), Cpn60 (ABUW_0918), RecA (ABUW_1748), and RpoD (ABUW_0862) were compared across the 292 genomes using screen_assembly v1.2.7 [21]. The search parameters used BLASTN v2.9.0 and were set to identify targets matching 80% sequence coverage and 80% sequence identity or above. Resulting hits were then translated into corresponding amino acid sequence. The sequence conservation of the analyzed genes was derived from a MUSCLE alignment [22] using Geneious prime [23] and the conservation percentages were derived from average pairwise identity.

2.2 Expression and purification of recombinant ZnuA and mutant variants from inclusion bodies

Recombinant ZnuA (residues 20 – 268) was cloned from *A. baumannii* AB5075_UW genomic DNA (ABUW_3740) into pET-30a(+) vector via Gibson assembly. Mutant variants were generated using site-directed mutagenesis (QuickChange Lighting Kit, Agilent Technologies) using primers described in (**Table S1**). Wild-type ZnuA and mutant variants were overexpressed in *E. coli* LEMO21(DE3) with their respective expression construct (**Table S2**). Bacterial cultures were grown in Overnight Express Instant TB medium (Merck) supplemented with 10% glycerol and 100 $\mu g.mL^{-1}$ kanamycin for 18 h at 26 °C. Cultures were harvested through centrifugation at 6,000 × *g* for 30 min, and pellets were resuspended in 50 mM 3-(*N*-morpholino)propanesulfonic acid (MOPS) (pH 7.8), 200 mM NaCl, 20% glycerol, and 15 mM imidazole buffer. Cells were homogenized and then lysed using mechanical disruption at 30 kpsi in a cell disruptor (Constant Systems) and were centrifugated at

120,000 × *g* at 4 °C for 1 h to isolate cellular debris. Cellular debris containing the inclusion bodies was then washed twice with washing buffer A (50 mM MOPS [pH 7.8], 2 M urea, 200 mM NaCl, 1 mM ethylenediaminetetraacetic acid (EDTA), 1% Triton), and twice with washing buffer B (50 mM MOPS [pH 7.8], 200 mM NaCl, 1 mM EDTA) via centrifugation at 6,000 × *g* for 10 min. The supernatant was then discarded, and the pellets were stored at – 80 °C for future experiments. Inclusion bodies were solubilized in urea buffer A (50 mM MOPS [pH 7.8], 8 M urea, 200 mM NaCl) overnight with agitation at room temperature. The mixture was harvested by centrifugation at 120,000 × *g* at 4 °C for 1 h, followed by filtration through a 0.4 µm filter (Sartorius). Dodecahistidine-tagged ZnuA recovered from the inclusion bodies was purified under denaturing conditions by immobilized metal ion affinity chromatography (IMAC) as described previously [24].

2.3 Refolding of purified denatured ZnuA proteins and cleavage of dodecahistidine tag

Purified, denatured wild-type and variant ZnuA proteins were refolded by dialysis in refolding buffer (50 mM MOPS, 0.25 M L-arginine, 500 mM NaCl, 1 mM EDTA) using a 20 kDa molecular weight-cutoff (MWCO) membrane (Slide-A-Lyzer, ThermoFisher Scientific) for 24 h at 4 °C. Insoluble material was removed from the refolded, recombinant ZnuA proteins by ultracentrifugation, 120,000 × *g* at 4 °C for 1 h. The dodecahistidine tag was removed by enzymatic digestion using a recombinant histidine-tagged human rhinovirus 3C protease for 1 h at a ratio of 1:20 protease to recombinant ZnuA proteins at 4 °C with stirring. The sample was reverse purified with recombinant, tag-cleaved ZnuA proteins eluted from a 5 mL HisTrap column (Cytiva). Removal of the dodecahistidine tag was confirmed by SDS-PAGE analyses.

2.4 Differential scanning fluorimetry

Metal-free, recombinant tag-cleaved ZnuA and ZnuA variants (10 µM) were incubated with 10-fold molar excess of the first-row transition metal ions [Mn(II), Fe(II), Co(II), Ni(II), Cu(II), Zn(II)] at room temperature in the presence of 5 × SYPRO Orange (ThermoFisher Scientific). Samples were

subjected to thermal unfolding and analyzed using QuantStudio Flex 7 Real-Time PCR system (ThermoFisher Scientific) at a heating rate of 0.3 °C.s^{-1}. Fluorescence data were collected at excitation 470 nm/emission 570 nm for buffer only, metals only, protein with and without metal treatment. After subtraction of background fluorescence of the buffer, the first derivative of the fluorescence data was determined and analyzed using GraphPad Prism (Version 8) to determine the inflection point of the melting transition (T_m). The metal-free protein showed a minor species (46.0 ± 3.0 °C) and a major species (53.7 ± 1.2 °C), with the major species used to determine the ΔT_m. Although clarification by ultracentrifugation and/or filtration prior to differential scanning fluorimetry (DSF) did not prevent the metal-free sample T_m complexity, addition of metals ions produced a single species. Data from at least three independent experiments were used to determine the ΔT_m ± S.D. of the wild-type ZnuA and ZnuA variants. Statistical significance was determined using one-way ANOVA using a Tukey post-test.

2.5 Metal-binding experiments

Metal-free ZnuA (30 µM) was incubated with 10-fold molar excess of the first-row transition metal ions [Mn(II), Fe(II), Co(II), Ni(II), Cu(II), Zn(II)] for 1 h with agitation in a total of 2 mL at 4 °C. Metal-binding assays were performed in binding assay buffer (50 mM MOPS [pH 7.8], 200 mM NaCl). Following incubation, unbound metal ions were removed by buffer exchange into the binding assay buffer using a PD10 column (GE Healthcare). Solutions of metal-loaded recombinant ZnuA were prepared in 3.5% HNO_3 and boiled at 98 °C for 15 min. Samples were then centrifuged for 30 min at 20,000 × *g*, and the supernatant was analyzed using inductively coupled plasma-mass spectrometry (ICP-MS) to determine the metal:protein molar ratio [25, 26].

2.6 Competitive Zn(II) binding assays

Affinity measurement experiments were conducted by measuring the fluorescence of Mag-Fura-2 (150 nM) (ThermoFisher Scientific) saturated with Zn(II) in response to titration of metal-free protein

at (excitation 340 nm/emission 510 nm), using the CLARIOstar Plus spectrophotometer (BMG Labtech) [11]. Five technical replicates were measured for each sample in a black half-volume 384-well microtiter plate (Greiner Bio One), using a Chelex-100 treated 50 mM MOPS (pH 7.8) 200 mM NaCl buffer. Fluorescence values were analyzed in GraphPad Prism (Version 8) by a one-site non-linear fit model, using the experimentally derived K_D of Mag-Fura-2 (47 nM) to derive the K_D for Zn(II) binding by ZnuA.

2.7 Structure determination by X-ray crystallography

Recombinant ZnuA was concentrated to approximately 10 mg.mL^{-1} in centrifugal filter units (Amicon MWCO 30 kDa, Millipore). Crystals were obtained at 20 °C using the hanging drop vapor diffusion technique in 0.1 M citrate (pH 7.0), 30% (v/v) polyethylene glycol 6000, and 1 M LiCl. Crystals were mounted onto Cryoloops (Hampton Research) and briefly soaked in Paratone-N (Hampton Research) prior to flash-cooling in liquid nitrogen. X-ray diffraction data were collected at the Australian Synchrotron MX2 beamline [27]. Diffraction data were indexed and integrated using *XDS* [28] and scaled and merged using *Aimless* [29]. The structure was determined using the molecular replacement in *Phenix.Phaser* [30], using a search model generated *in silico* by AlphaFold2 [31]. An initial model was built in *Phenix.AutoBuild* [32]. The following residues could not be modeled due to the lack of electron density and are presumably disordered: Ser33-Gln38, Ser153-Ser154 and Thr216-Gln221. The structures was refined iteratively using *Phenix.Refine* [33] and manually modified in *COOT* [34]. The coordinates and structure factors have been deposited in the Protein Data Bank (PDB ID 7SHJ).

2.8 Molecular dynamics simulations

Chain A in the crystal structure of metal-free ZnuA was used as the starting structure for the simulations. All crystallographic waters and sodium were removed. The residues missing in the model were reconstructed using the 'Builder' tool in PyMol [35]. All His residues were protonated based on hydrogen bonding potential with surrounding residues. For all simulation systems, the protein was

placed in a rectangular box, solvated with water molecules and Na^+ ions were added to neutralize the charge on the protein. Additional Na^+ and Cl^- ions were added to obtain a final ionic strength of 100 mM NaCl. The system was energy-minimized using a steepest descent algorithm, followed by a 5-ns NVT run and a 5-ns NPT run where the protein backbone atoms were position-restrained (posre) with a force constant of 500 kJ $mol^{-1}.nm^{-2}$. The output from the NPT posre run was used as the starting structure for the production runs. Three independent simulations of 750 ns each were carried out using different seeds to generate starting velocities.

All simulations were carried out using the GROMACS package version 5.0.1 [36, 37] in conjunction with the GROMOS 54a7 force field [38] for protein and the simple point charge (SPC) model for water [39]. Simulations were carried out under periodic boundary conditions with at least 1.2 nm between the protein and the box wall. For non-bonded interactions, the van der Waals and short-ranged interactions were treated using a Verlet scheme with cut-offs 1.0 nm and 1.2 nm, respectively. Long-range electrostatics were treated using a PME with grid spacing 0.16 and a cubic interpolation of 4. The LINCS constraints algorithm was used. Temperature was kept at 298 K using a V-rescale thermostat and a time constant of 0.1 ps. A separate coupling groups was used for the protein and water/ions. Pressure was kept at 1 bar using a Parrinello-Rahman barostat with isotropic coupling and a time constant of 2.0. Simulations were carried out using a 2-fs time step. Initial velocities were randomly assigned from Maxwellian distributions at 298 K. Configurations were saved every 100 ps for analysis. Analysis was carried out using GROMACS tools and the python library MDAnalysis [40]. Unless otherwise stated, only the last 250 ns of each trajectory was used for analysis and independent simulations for a given system were analyzed separately. All images were prepared using VMD [41]. Cluster analysis was carried out using the algorithm of Daura *et al.* [42], implemented in GROMACS tools. A backbone neighbor root-mean-square deviation (RMSD) cut-off of 2.5 Å was used. From each of the simulations, the most dominant conformation was used.

2.9 Data availability

The accession code for the structure deposited in the Protein Data Bank is 7SHJ.

3. RESULTS AND DISCUSSION:

3.1 ZnuA and the zinc acquisition machinery are conserved in *A. baumannii* species

The conservation and prevalence of *A. baumannii* ZnuA and the other components of the Zn(II) acquisition system were investigated within a global database of 292 genome sequences (**Table S3**). This was performed by comparing the amino acid sequences of the ABC permease components, ZnuA (ABUW_3740), ZnuB (ABUW_3743), and ZnuC (ABUW_3742), the outer membrane receptor ZnuD1 (ABUW_0600), the metallochaperone ZigA (ABUW_0073), and the metalloregulator ZuR (ABUW_3741) from 292 publicly available *A. baumannii* genomes, which represents isolates from environmental and clinical niches [20]. This analysis revealed that the Zn(II) acquisition machinery as defined by carriage of all 6 genes were present in >98% of *A. baumannii* genomes and exhibited >97% amino acid conservation (**Table 1**). Notably, ZnuA had sequence conservation of 99.9%, which is comparable to the multilocus sequence typing proteins GltA (ABUW_0867), GyrB (ABUW_0004), Cpn60 (ABUW_0918), RecA (ABUW_1748), RpoD (ABUW_0862) (**Table 1**). Intriguingly, although *A. baumannii* ZnuA is highly conserved within *A. baumannii* strains, it has relatively low sequence homology (<30%) to the structurally and functionally characterized members of the cluster A-I family of Zn(II)-specific SBPs. The protein is most closely related to ZnuA from *Yersinia pestis* (25.1% sequence identity across 338 amino acid residues) and *E. coli* (24.5% sequence identity across 318 amino acid residues) (**Fig. 1A**) [43, 44]. ZnuA orthologs typically coordinate a single Zn(II) ion at the metal-binding site via three Nε2 atoms, contributed His side chains, and an O atom, contributed by either a carboxylate residue or water molecule. Alignment of *A. baumannii* ZnuA with other Zn(II)-specific SBPs identified three putative histidine residues as being highly conserved, His41, His109, and His170 (**Fig. 1B**). These putative Zn(II)-coordinating His residues were also invariant, i.e. 100% conservation, in all *A. baumannii* species analyzed. However, no conserved carboxylate residue was identified in *A. baumannii* ZnuA by comparison with other cluster A-I SBPs. This may suggest that Zn(II) retains coordination with a water molecule at the metal-binding site, as observed for ZnuA from *Synechocystis* sp. [45], or that the coordinating carboxylate

residue is contributed by a distinct region not observed in other characterized structures. *A. baumannii* ZnuA also lacks a histidine-rich region, which is frequently observed in other Zn(II)-specific SBPs (**Fig. 1B**). This region has been implicated in aiding SBP sampling of bulk solvent for Zn(II) ions [45, 46], although the length varies considerably and can span from 12 residues [47] to 50 residues [48]. Nevertheless, some Zn(II) specific SBPs, such as *S. pneumoniae* AdcAII [49], also lack this region, suggesting that its presence is not a prerequisite for function.

Collectively, these findings show that the Zn acquisition machinery is highly conserved in diversity of *A. baumannii* genomes analyzed. Further, the amino acid conservation of ZnuA indicates that mutations are poorly tolerated, suggesting that these rarely confer beneficial properties, with respect to the physiological function in ligand binding and/or interaction with ZnuBC.

3.2 *A. baumannii* ZnuA can interact with zinc and cobalt

To further investigate *A. baumannii* ZnuA a recombinant C-terminal dodecahistidine-tagged variant that lacked the predicted signal peptide sequence was generated (ABUW_3740; residues 20 to 268). Recombinant ZnuA was expressed, the C-terminal dodecahistidine-tag cleaved and the protein reverse-purified and analyzed by size-exclusion chromatography. The recombinant protein had an estimated a relative molecular mass of 28.5 kDa, which compared favorably to the theoretical mass for monomeric species of 29.9 kDa (**Fig. 2A,B**).

The interaction of recombinant, tag-cleaved *A. baumannii* ZnuA with the first-row *d*-block elements manganese (Mn), iron (Fe), cobalt (Co), nickel (Ni), copper (Cu), and Zn was then assessed by DSF [50]. Recombinant ZnuA showed significant increases in thermostability, as defined by the apparent melting transition (T_m) temperature upon interaction with Co(II) and Zn(II) (**Table 2**). The *d*-block elements Mn(II), Fe(II), Ni(II) and Cu(II), were not observed to induce significant changes in protein thermostability (**Table 2**). A limitation of DSF analyses is that it does not directly measure metal-binding. Ligand-induced increases in thermostability are inferred to reflect the formation of a more stable complex and in cluster A-I SBPs are indicative of conformational changes. Therefore, to

complement the DSF analyses, we also performed *in vitro* metal-binding experiments, to ascertain which *d*-block elements could interact with *A. baumannii* ZnuA. Metal-free recombinant ZnuA was incubated with a 10-fold molar excess of each *d*-block element, followed by desalting, to remove unbound metal ions. Analysis of recombinant ZnuA showed that it bound 1.07 ± 0.4 mole of Zn(II) per mol of protein (S.E.M.; **Fig. 2C**). Thus, the *in vitro* Zn(II) binding data are consistent with the observation of a single high-affinity site within the structure of *A. baumannii* ZnuA, while the DSF analyses support the inference that Zn(II) is the physiological ligand.

Recombinant ZnuA was also observed to bind sub-stoichiometric amounts of Fe(II), Co(II) and Ni(II) and an excess of Cu(II) (~ 1.5 mole Cu(II) per mole ZnuA). However, Fe(II), Ni(II) and Cu(II) were not associated with T_m changes in recombinant ZnuA. This may be due to inability of these metal ions to interact with the primary metal binding site, poor affinity of these cations for the metal binding site leading to dissociation during desalting, failure of the metal-protein interaction to induce a transition to a more stable metal-protein complex, or some combination thereof. The first inference is potentially supported, at least in part, by the molar excess of Cu(II) associated with ZnuA. The putative composition of the metal-binding site of *A. baumannii* ZnuA, comprised by three histidine residues, is rarely observed in Cu-coordinating structures within the PDB [51]. We speculate that some or all of the ZnuA-bound Cu(II) was adventitiously associated with surface exposed sulfur-containing residues, such as methionine 208 and cysteine 209. Although future experiments would be required to validate this inference, metal ions interacting with secondary sites on the surfaces of SBPs have been reported [52-54]. However, it is important to note that the role of these secondary metal ion interaction sites remains unclear, as they do not appear to facilitate entry of metal ions into the ABC transporter [54].

In this work, Co(II) was the only non-cognate metal observed to bind and induce a T_m shift. The sub-stoichiometric association of Co(II) with ZnuA in the metal binding assay suggests that the protein has a poor affinity for the metal and/or that the metal is incapable of inducing a transition to a closed SBP conformation. Irrespective of the mechanistic basis, access to the metal binding site by

bulk solvent could promote dissociation of Co(II) during the desalting step of the protein-metal quantitation analytical process. Despite the capacity of Co(II) to interact with *A. baumannii* ZnuA, it is unclear whether it could be transported by the ZnuBC transporter. Recent structural and mechanistic studies of the related metal-specific ABC permease PsaBC from *Streptococcus pneumoniae* revealed a putative metal-binding site within the translocation pathway that was crucial for cation import [55]. The transmembrane binding site was essential for cation translocation and appeared to employ coordination chemistry. This mechanism was suggested to prevent translocation of non-cognate cations, such as Co(II). The coordination site residues are conserved within *A. baumannii* ZnuB (Asp39 and His43), although whether it serves in cation selectivity remains to be determined. It is also important to note that the acquisition of ionic Co(II) in prokaryotes is primarily mediated by energy-coupling factor (ECF) transporters, a distinct subgroup of bacterial ABC transporters [56, 57]. The Co(II)-specific ECF transporters employ the integral membrane protein CbiN that confers specificity for Co(II) ions in the $CbiMQO_2$ transporter [56, 57]. Thus, under physiological conditions it is reasonable to speculate that CbiN scavenges labile Co(II), thereby reducing potential interaction with ZnuA. A further consideration is that within the context of host niches, it is highly unlikely Co(II) would compete with Zn(II) for *A. baumannii* ZnuA, as Co is predominantly present as the metal chelate cobalamin. Collectively, this combination of factors may have obviated evolutionary selective pressure to evolve a capacity to discriminate between Zn(II) and Co(II) ions in ZnuA. We next sought to characterize the structural properties of *A. baumannii* ZnuA.

3.3 Structural analysis of *A. baumannii* ZnuA

Recombinant *A. baumannii* ZnuA was used in crystallographic trials, with and without Zn(II). Despite multiple attempts, Zn(II)-bound ZnuA did not yield crystals of sufficient quality for X-ray diffraction. Nevertheless, crystals of metal-free ZnuA were obtained and diffraction data was collected to 2.1 Å resolution. Two ZnuA molecules are present in each asymmetrical unit. Residues 1, 37-45, 159-160, 222-227 in chain A and 1, 37-45, 160-163, 192-193, 220-224 in chain B were not modelled due to

lack of interpretable electron density in those regions. Crystallographic and refinement statistics are summarized in **Table S4**. *A. baumannii* ZnuA adopts a canonical cluster A-I SBP fold that is comprised by two globular domains, henceforth referred to as the N- and C-terminal domains, that each contain a 4-α-helical bundle (α1-4, α6-9) with a 4-stranded β-sheet (β1-4, β5-8). The two domains are connected by a long helical linker (α5) (**Fig. 3**), with the metal binding site predicted to be located at the interface between the two domains. The putative Zn(II)-coordinating residue, His41, is predicted to be located in the amino-terminal (N-terminal) domain loop α2β2, but could not be modelled due to poorly resolved electron density of this region. His109 is located at the base of the metal binding site contributed by a short loop, while His170 is in the C-terminal domain loop α6β5 (**Fig. 3**). The structure of *A. baumannii* ZnuA represents an open, metal-free conformation, wherein the putative metal binding site is fully exposed to bulk solvent.

A. baumannii ZnuA was then compared with crystal structures of open-state cluster A-I SBPs of *E. coli* ZnuA (PDB 2PS3) [43], *Salmonella enterica* ZnuA (PDB 2XH8) [58], *Synechocystis* 6803 ZnuA (PDB 2OV1) [46], *Paracoccus denitrificans* AztC (PDB 5W56) [59], and *S. pneumoniae* AdcAII (PDBs 7LM5, 7LM6) [11] (**Fig. 4**). This analysis revealed that the proteins adopted similar conformations, with root mean square deviations of the Cα protein backbones (Cα-RMSD) not exceeding 3.0 Å (**Table S5**). However, distinct differences between *A. baumannii* ZnuA and the representative cluster A-I SBPs were observed. Notably, loop α2β2 in the N-terminal domain, which harbors the putative Zn(II)-coordinating residue His41, is largely disordered, indicating that this loop has high mobility in the absence of a metal ligand. This observation contrasts starkly with metal-free ZnuA from other bacterial species, wherein loop α2β2 frequently adopts a stabilized, but distinct conformation. The disorder observed for loop α2β2 in structural analysis of *A. baumannii* ZnuA closely resembles observations of this region in AdcA and AdcAII, the Zn(II)-recruiting SBPs of *Streptococcus pneumoniae* [9, 11]. In *S. pneumoniae* AdcA, loop α2β2 was predicted to be disordered in the absence of Zn(II)-binding [9], and could not be modelled in the His65 mutant of AdcAII [11]. Loop α2β2 in AdcA has been proposed to serves as a “trap-door” component of the metal-binding

mechanism and has a crucial role in controlling solvent access to the Zn(II)-binding site and Zn(II) uptake. Here, we speculate that loop α2β2 may serve a similar role in *A. baumannii* ZnuA. Binding of a Zn(II) ion by loop α2β2 would enable the position of the mobile region to be stabilized and, upon coordination of the Zn(II) by other binding site residues, enable conformational changes that reduce bulk solvent access to the metal-binding site. Substantial conformational diversity was also observed in the C-terminal domain of *A. baumannii* ZnuA. In contrast to almost all other cluster A-I SBPs structures in their metal-free states, α8 in *A. baumannii* ZnuA is disordered. In addition, α7 and the 4-stranded β-sheet show an approximate 2.4 Å shift relative to the same structural elements in other SBP crystal structures. The domain-linking helix α6 is also shorter than the comparable region observed in other cluster A-I SBPs with the region connecting the C-terminal domain, residues 150-156, forming a loop, as opposed to being part of the domain-linking helix observed in all other SBPs. Whether the shorter length of this helix has a mechanistic effect on Zn(II)-binding remains to be investigated. Overall, the structural analysis of *A. baumannii* ZnuA reveals further diversity and complexity within the conformational landscape of open-state metal-recruiting SBPs.

To gain further insight into the structure of *A. baumannii* ZnuA molecular dynamics (MD) simulations were performed. The missing sections of the crystal structure were modelled as follows: residues 37-45 and 222-227 (the missing section at the end of the domain-linking helix α5), were modelled as loops; residues 156-162 was modelled as an α-helix. The SBP with the reconstructed sections was then used as a starting point for three independent, 750-ns long MD simulations of which the last 250 ns of each simulation were used for analysis. In all three simulations, the overall fold of the protein remained stable (**Fig. 5A**) with an average Cα-RMSD of 1.8 Å ± 0.1 with respect to the starting structure. As suggested by the crystal structure, domain-linking helix α5 ends at 150 and the remaining residues before the β-strand form a loop. This structure is confirmed by the absence of stable hydrogen bonds in the main chain between 150 and 156. The analysis suggests that *A. baumannii* ZnuA is unlikely to employ a rotation of the C-terminal domain for ligand binding, as observed in *S. pneumoniae* PsaA [60]. In reconstructed ZnuA, α7 was modelled as an α-helix and

remained stable in two (of the three) simulations. In one simulation, the first turn (residues 228-230) unfolded, while residues 224-228 remained in helical form. In all simulations, the loop formed by residues 218-222 that connects the preceding β-strand to α7 is mobile, such that it affects the position of α7 with respect to the plane running along the domain linking helix. We speculate that this motion and the instability of structural elements within α7 contributed to the lack of interpretable diffraction electron density within this region of the crystal structure.

The MD simulations also enable further investigation of the loops that contain the putative Zn(II)-coordinating His residues. Loop α2β2, which contains His41, showed the highest mobility and samples various conformations (**Fig. 5B**). As a result, the position of His41 with respect to the central Zn(II)-binding site varied substantially over the course of the simulations (**Fig. S1**). We predict that the mobility of loop α2β2 would be reduced in the Zn(II)-bound state. The short loop that contains His109, and loop α6β5, which contains His170, show less mobility and adopt the same dominant conformation in *A. baumannii* ZnuA (**Fig. 5B, Fig. S1**). Accordingly, the positions of His109 and His170 are relatively stable with respect to the Zn(II)-binding site. Further analysis showed that the solvent accessibility of these loops fluctuates around the respective values observed in the crystal structure. In summary, the MD simulations of reconstructed ZnuA indicate that the overall fold of the metal-free SBP is stable, but regions of mobility are present within it, such as loop α2β2, and these may contribute to the ligand recruiting mechanism.

3.4 Putative metal-binding site histidine residues are essential for ZnuA function

The role(s) of the putative metal-coordinating residues were then investigated by generating ZnuA point mutants lacking one of the three histidine residues. The resultant ZnuA variants $ZnuA_{H41A}$, $ZnuA_{H109A}$ and $ZnuA_{H170A}$ were expressed and purified using the framework established for wild-type recombinant, tag-cleaved ZnuA. The affinity of wild-type ZnuA and the mutant variants was then determined using a competitive binding assay. The derived K_D of recombinant ZnuA for Zn(II) was determined to be 87 ± 2 nM (S.E.M.; **Table 3**). This value is within the range reported for other

Zn(II)-specific SBPs [9, 10, 61, 62]. The ZnuA variants all had reduced affinity for Zn(II), but the extent varied substantially (**Table 3**). The overall order of Zn(II) affinity observed for the proteins was ZnuA > $ZnuA_{H109A}$ > $ZnuA_{H41A}$ > $ZnuA_{H170A}$ (highest to lowest).

The impact of the mutations on protein thermostability was next assessed by DSF analyses (**Table 4**). The *A. baumannii* ZnuA variant proteins showed a minor reduction in overall thermostability by comparison to the wild-type protein (**Table 2**), although this was only statistically significant for $ZnuA_{H170A}$ (*P* value = 0.0226; one-way ANOVA with Tukey post-test). The results strongly suggest that the point mutations did not perturb global protein structure and that the variant proteins were stable for further investigation of protein-metal complex interactions. DSF analysis of the *A. baumannii* ZnuA variant proteins revealed that substitution of any of the metal-binding site histidine residue abrogated the Zn(II) and Co(II) induced T_m shifts observed in the wild-type protein (**Tables 2,4**). The results indicate that residues His41, His109, and His170 all serve crucial roles in the stabilization of the *A. baumannii* ZnuA-metal complex.

Given the disruption in thermostabilization of cognate ligand binding observed by DSF analyses, the recombinant ZnuA variants were analyzed for *in vitro* zinc-binding capacity to assess whether this was also perturbed by the loss of the binding-site His residues. We observed that $ZnuA_{H41A}$ was not impacted for Zn(II)-binding, whereas $ZnuA_{H109A}$ and $ZnuA_{H170A}$ showed significant reductions in Zn(II) binding capacity, relative to the wild-type protein (**Fig. 6**). When considered in the context of the MD simulation analyses, the DSF data suggest that the metal-binding site is partially preformed by His109 and His170, which are relatively static in the protein structure and exposed to bulk solvent. By contrast, we predict that the mobile α2β2 loop, which contains His41, is stabilized upon Zn(II)-binding. Thus, these findings suggest a Zn(II)-binding mechanism wherein His109 and His170 serve to stabilize Zn(II) interaction with the base of the metal-binding site, while His41, upon interaction of Zn(II), serves to reduce the mobility of loop α2β2, closing it over the binding site and reducing access to bulk solvent. The crucial role of His41 in ZnuA function is also supported by phenotypic studies of *A. baumannii* ATCC 1797 [4]. That work showed ectopic

expression of the *znuA*$_{His41A}$ variant in the *A. baumannii* ATCC 1797 Δ*znuA* background was incapable of rescuing growth in Luria broth treated with 30 μM *N,N,N′,N′*-tetrakis(2-pyridinylmethyl)-1,2-ethanediamine (TPEN), a preferential Zn(II)-chelator [4]. However, whether this was due to reduced affinity of ZnuA variant for Zn(II), the inability to stabilize loop α2β2 and preventing TPEN chelation of bound Zn(II), and/or disruption of the ZnuA-ZnuBC interface, remains to be determined. Further investigations into the metal-binding dynamics of *A. baumannii* ZnuA and the structure of Zn(II)-bound wild-type SBP and mutant derivatives would address the veracity of this mechanistic model.

4. CONCLUSIONS

This study provides new insights into the structure and mechanistic aspects of *A. baumannii* ZnuA. This Zn(II)-recruiting protein is a highly conserved component of the essential acquisition machinery present in diverse *A. baumannii* strains. The high-resolution structure of open, metal-free state of ZnuA reveals that the N-terminal loop α2β2, which contains the Zn(II)-binding His41 residue, is a region of dynamic mobility in the absence of ligand. This region appears to play a crucial role in occluding Zn(II) at the metal-binding site from bulk solvent and thereby promotes efficacious import via the ZnuBC transporter. The essentiality of Zn(II) for bacterial pathogens makes it a highly attractive target for antimicrobial development. The data herein provides a foundation for future structure-based therapeutic development studies to target *A. baumannii* ZnuA-mediated Zn(II) acquisition.

TABLES

Table 1. Conservation and prevalence of known *A. baumannii* Zn(II) acquisition proteins within 292 genome sequences.

Zn(II) acquisition proteins	**Conservation (%)**	**Prevalence (%)**
ABUW_3740 (**ZnuA**)	99.9	99.3
ABUW_3743 (**ZnuB**)	99.4	99.6
ABUW_3742 (**ZnuC**)	99.6	99.6
ABUW_3741 (**ZuR**)	99.9	100
ABUW_0600 (**ZnuD1**)	97.9	98.2
ABUW_0073 (**ZigA**)	99	98.9
MLST proteins	**Conservation (%)**	**Prevalence (%)**
ABUW_0876 (**GltA**)	100	100
ABUW_1083 (**GyrB**)	99.8	100
ABUW_0918 (**Cpn60**)	100	100
ABUW_1748 (**RecA**)	100	99.6
ABUW_0862 (**RpoD**)	100	100

Table 2. Effect of divalent cations on the melting temperature of wild type ZnuA

Metal Treatment	T_m (°C)†	ΔT_m
Metal-free ZnuA	55.5 ± 1.2	
ZnuA 1:10 Mn(II)	55.3 ± 0.9	- 0.2
ZnuA 1:10 Fe(II)	53.8 ± 0.9	- 1.7
ZnuA 1:10 Co(II)	58.8 ± 1.3	+ 3.3‡
ZnuA 1:10 Ni(II)	57.4 ± 0.5	+ 1.9
ZnuA 1:10 Cu(II)	55.3 ± 1.9	- 0.2
ZnuA 1:10 Zn(II)	63.8 ± 0.8	+ 8.3‡

† Values shown represent the mean and standard deviation from at least three independent measurements.

‡ Statistically significant difference compared to metal-free protein T_m (one-way ANOVA with Tukey post-test).

Table 3. Effect of metal binding site mutations on *in vitro* Zn(II) binding

Protein	**K_D (nM)**
ZnuA	87 ± 2
$ZnuA_{H41A}$	342 ± 125
$ZnuA_{H109A}$	114 ± 33
$ZnuA_{H170A}$	658 ± 103

Table 4. Effect of divalent cations on the melting temperature of ZnuA variant proteins

Metal Treatment	$ZnuA_{H41A}$ T_m (°C)†	$ZnuA_{H41A}$ ΔT_m	$ZnuA_{H109A}$ T_m (°C)†	$ZnuA_{H109A}$ ΔT_m	$ZnuA_{H170A}$ T_m (°C)†	$ZnuA_{H170A}$ ΔT_m
Metal-free ZnuA	53.5 ± 0.1		53.2 ± 0.1		52.7 ± 0.4	
ZnuA 1:10 Mn(II)	54.3 ± 1.0	+ 0.8	52.1 ± 0.8	- 1.1	52.5 ± 0.6	- 0.2
ZnuA 1:10 Fe(II)	55.0 ± 0.2	+ 1.5	52.4 ± 0.5	- 0.8	53.1 ± 0.6	+ 0.4
ZnuA 1:10 Co(II)	54.8 ± 1.1	+ 1.3	52.9 ± 0.7	- 0.3	52.9 ± 0.5	+ 0.2
ZnuA 1:10 Ni(II)	56.3 ± 0.4	+ 2.8‡	53.3 ± 0.7	+ 0.1	53.7 ± 0.1	+ 1.0
ZnuA 1:10 Cu(II)	52.5 ± 0.8	- 1.0	52.4 ± 0.4	- 0.8	52.0 ± 0.0	- 0.7
ZnuA 1:10 Zn(II)	55.2 ± 1.2	+ 1.7	54.4 ± 1.8	+ 1.2	51.9 ± 3.5	- 0.8

† Values shown represent the mean and standard deviation from at least three independent measurements.

‡ Statistically significant difference compared to metal-free protein T_m (one-way ANOVA with Tukey post-test).

FIGURE LEGENDS

Figure 1. Sequence homology and alignment of *A. baumannii* ZnuA in comparison to cluster A-I Zn(II) SBPs

(**A**) Sequence percentage identity of characterized cluster A-I Zn(II) SBPs, compared to *A. baumannii* ZnuA. The numbers inside the boxes represent the sequence identity percentage. (**B**) Sequence comparison and alignment between *A. baumannii* ZnuA and Zn(II)-binding cluster A-I SBPs. The conserved His residues are highlighted in green and the His-rich loop highlighted in blue.

Figure 2. Purification of recombinant wild-type ZnuA from inclusion bodies

(**A**) Absorbance (280 nm) trace of recombinant ZnuA, analyzed by size exclusion chromatography using a Superdex 200 increase 10/300 GL column. The inset represents linear regression of protein molecular weight standard calibration. (**B**) Coomassie-stained 12.5% SDS-PAGE showing: lane 1, molecular weight standards with sizes indicated (left); and lane 2, peak eluent fraction from size exclusion column (A) with ZnuA indicated by an arrow. (**C**) *In vitro* metal-binding experiments of the metal-free ZnuA with *d*-block metal ions shown. Data represent the mean molar ratio of metal ions to ZnuA (± S.E.M.) from at least three independent biological experiments.

Figure 3. Crystal structure of *A. baumannii* ZnuA in the metal-free state

The structure of metal-free ZnuA (PDB ID 7SHJ) with the N- and C-terminal domains colored in green and yellow, respectively, and the domain-linking helix in magenta. The Zn(II)-coordinating residues His109 and His170 are shown in stick representation.

Figure 4. Structural comparisons of *A. baumannii* ZnuA with homologues in their metal-free states

Structural comparison of *A. baumannii* ZnuA (magenta) with (**A**) *E. coli* ZnuA (PDB ID 2PS3; yellow); (**B**) *S. enterica* ZnuA (PDB ID 2XH8; cyan); (**C**) *Synechocystis* 6803 ZnuA (PDB ID 2OV1;

light blue); (**D**) *P. denitrificans* AztC (PDB ID 5W56; grey); (**E**) *S. pneumoniae* AdcAII$_{H65A}$ (PDB ID 7LM5; light green); and (**F**) *S. pneumoniae* AdcAII$_{H205L}$ (PDB ID 7LM6; orange). The metal-coordinating residues of the respective structure are shown in stick representation. The α2β2 loop (denoted by arrow) and α8 regions, which are absent in the *A. baumannii* ZnuA crystal structure, and α7, which shifts relative to the same structural elements in other structures, are labeled.

Figure 5. MD simulations of reconstructed ZnuA

(**A**) Overlay of the metal-free ZnuA structure (PDB ID 7SHJ; magenta) with a representative structure from MD simulations of the reconstructed metal-free ZnuA structure (cyan). (**B**) MD simulations examining the mobility of the histidine-containing loops. A representative structure of the full-length, reconstructed ZnuA structure is shown in cyan and overlayed with 12 conformations of loops from the MD simulations: α2β2, which contains His41, shown in red; the short loop containing His109 shown in blue; and α6β5, which contains His170, shown in orange.

Figure 6. *In vitro* Zn(II) binding of wild-type ZnuA and mutant variants

In vitro Zn(II)-binding experiments of ZnuA and the mutant variants ZnuA$_{H41A}$, ZnuA$_{H109A}$, ZnuA$_{H170A}$. Data represent the mean molar ratio of ^{66}Zn to protein (± S.E.M.) from at least three independent biological experiments. Statistical significance was determined by performing a one-way ANOVA analysis with Bonferroni post-test.

ACKNOWLEDGEMENTS

We thank Dr Bart Eijkelkamp (Flinders University, Australia) for providing the AB5075_UW strain and for discussions. We also thank Prof. Eric Skaar and Laura Hesse (Vanderbilt University, USA) for discussions and feedback on the manuscript. We acknowledge use and thank the staff of the Australian Synchrotron MX beamlines and the UQ-ROCX (University of Queensland Remote Operation Crystallization and X-Ray Diffraction) Australian Microscopy & Microanalysis Research Facility at the Centre for Microscopy and Microanalysis, The University of Queensland.

FUNDING

This research was undertaken with the assistance of resources and services from the National Computational Infrastructure (NCI), which is supported by the Australian Government and by resources provided by The Pawsey Supercomputing Centre with funding from the Australian Government and the Government of Western Australia. This research was also undertaken using the LIEF HPC-GPGPU Facility hosted at the University of Melbourne. This Facility was established with the assistance of Australian Research Council (ARC) LIEF Grant LE170100200. This work was supported by the National Health and Medical Research Council (NHMRC) grants 1071659 to B.K., 1122582 to C.A.M., and 1180826 to B.K. and C.A.M. E.D. is a UTS Chancellor's Postdoctoral Fellow, B.K. is an ARC Laureate Fellow (FL180100109), and C.A.M. is an ARC Future Fellow (FT170100006). The content of this study is solely the responsibility of the authors and does not necessarily represent the official views of the funding bodies.

AUTHOR CONTRIBUTIONS

SA, MRD, BK, ED, and CAM designed the study. SA performed the biochemical and biophysical studies, with KG performing the ICP-MS analyses. SA, AH, and MRD performed the bioinformatic studies. ZL, TV, and BK performed the structural analyses. ED and SIH performed the molecular dynamics studies. SA wrote the first draft of the manuscript with specific sections contributed by ZL

and ED. CAM reviewed and revised the manuscript text. All authors read and approved the submitted version.

REFERENCES

[1] C. Andreini, L. Banci, I. Bertini, A. Rosato, J Proteome Res, vol. 5, 2006, pp. 3173-3178.

[2] C. Andreini, I. Bertini, G. Cavallaro, G.L. Holliday, J.M. Thornton, J Biol Inorg Chem, vol. 13, 2008, pp. 1205-1218.

[3] K. Hantke, Curr Opin Microbiol, vol. 8, 2005, pp. 196-202.

[4] L.E. Hesse, Z.R. Lonergan, W.N. Beavers, E.P. Skaar, Infect Immun, vol. 87, 2019, pp. e00746-00719.

[5] S. Lhospice, N.O. Gomez, L. Ouerdane, C. Brutesco, G. Ghssein, C. Hajjar, A. Liratni, S. Wang, P. Richaud, S. Bleves, G. Ball, E. Borezee-Durant, R. Lobinski, D. Pignol, P. Arnoux, R. Voulhoux, Sci Rep, vol. 7, 2017, pp. 17132.

[6] V.G. Pederick, B.A. Eijkelkamp, S.L. Begg, M.P. Ween, L.J. McAllister, J.C. Paton, C.A. McDevitt, Sci Rep, vol. 5, 2015, pp. 13139.

[7] R. Gabbianelli, R. Scotti, S. Ammendola, P. Petrarca, L. Nicolini, A. Battistoni, BMC Microbiol, vol. 11, 2011, pp. 36.

[8] S. Ammendola, P. Pasquali, C. Pistoia, P. Petrucci, P. Petrarca, G. Rotilio, A. Battistoni, Infect Immun, vol. 75, 2007, pp. 5867-5876.

[9] Z. Luo, J.R. Morey, E. Deplazes, A. Motygullina, A. Tan, K. Ganio, S.L. Neville, N. Eleftheriadis, M. Isselstein, V.G. Pederick, J.C. Paton, T. Cordes, J.R. Harmer, B. Kobe, C.A. McDevitt, mBio, vol. 12, 2021, pp. e01958-01920.

[10] C.D. Plumptre, B.A. Eijkelkamp, J.R. Morey, F. Behr, R.M. Counago, A.D. Ogunniyi, B. Kobe, M.L. O'Mara, J.C. Paton, C.A. McDevitt, Mol Microbiol, vol. 91, 2014, pp. 834-851.

[11] M.L. Zupan, Z. Luo, K. Ganio, V.G. Pederick, S.L. Neville, E. Deplazes, B. Kobe, C.A. McDevitt, Front Cell Infect Microbiol, vol. 11, 2021, pp. 729981.

[12] E. Tacconelli, E. Carrara, A. Savoldi, S. Harbarth, M. Mendelson, D.L. Monnet, C. Pulcini, G. Kahlmeter, J. Kluytmans, Y. Carmeli, M. Ouellette, K. Outterson, J. Patel, M. Cavaleri, E.M. Cox,

C.R. Houchens, M.L. Grayson, P. Hansen, N. Singh, U. Theuretzbacher, N. Magrini, W.H.O.P.P.L.W. Group, Lancet Infect Dis, vol. 18, 2018, pp. 318-327.

[13] M.I. Hood, B.L. Mortensen, J.L. Moore, Y. Zhang, T.E. Kehl-Fie, N. Sugitani, W.J. Chazin, R.M. Caprioli, E.P. Skaar, PLoS Pathog, vol. 8, 2012, pp. e1003068.

[14] B.L. Nairn, Z.R. Lonergan, J. Wang, J.J. Braymer, Y. Zhang, M.W. Calcutt, J.P. Lisher, B.A. Gilston, W.J. Chazin, V. de Crecy-Lagard, D.P. Giedroc, E.P. Skaar, Cell Host Microbe, vol. 19, 2016, pp. 826-836.

[15] B.L. Mortensen, S. Rathi, W.J. Chazin, E.P. Skaar, J Bacteriol, vol. 196, 2014, pp. 2616-2626.

[16] S.F. Alquethamy, F.G. Adams, V. Naidu, M. Khorvash, V.G. Pederick, M. Zang, J.C. Paton, I.T. Paulsen, K.A. Hassan, A.K. Cain, C.A. McDevitt, B.A. Eijkelkamp, ACS Infect Dis, vol. 6, 2020, pp. 150-158.

[17] S.F. Alquethamy, M. Khorvash, V.G. Pederick, J.J. Whittall, J.C. Paton, I.T. Paulsen, K.A. Hassan, C.A. McDevitt, B.A. Eijkelkamp, Int J Mol Sci, vol. 20, 2019, pp. 575.

[18] S.F. Alquethamy, F.G. Adams, R. Maharjan, N.N. Delgado, M. Zang, K. Ganio, J.C. Paton, K.A. Hassan, I.T. Paulsen, C.A. McDevitt, A.K. Cain, B.A. Eijkelkamp, Appl Environ Microbiol, vol. 87, 2021, pp. e0171821.

[19] G.H. Scheepers, A.N.J.A. Lycklama, B. Poolman, FEBS Lett, vol. 590, 2016, pp. 4393-4401.

[20] J.J. Davis, A.R. Wattam, R.K. Aziz, T. Brettin, R. Butler, R.M. Butler, P. Chlenski, N. Conrad, A. Dickerman, E.M. Dietrich, J.L. Gabbard, S. Gerdes, A. Guard, R.W. Kenyon, D. Machi, C. Mao, D. Murphy-Olson, M. Nguyen, E.K. Nordberg, G.J. Olsen, R.D. Olson, J.C. Overbeek, R. Overbeek, B. Parrello, G.D. Pusch, M. Shukla, C. Thomas, M. VanOeffelen, V. Vonstein, A.S. Warren, F. Xia, D. Xie, H. Yoo, R. Stevens, Nucleic Acids Res, vol. 48, 2020, pp. D606-D612.

[21] M.R. Davies, L. McIntyre, A. Mutreja, J.A. Lacey, J.A. Lees, R.J. Towers, S. Duchene, P.R. Smeesters, H.R. Frost, D.J. Price, M.T.G. Holden, S. David, P.M. Giffard, K.A. Worthing, A.C. Seale, J.A. Berkley, S.R. Harris, T. Rivera-Hernandez, O. Berking, A.J. Cork, R. Torres, T. Lithgow, R.A. Strugnell, R. Bergmann, P. Nitsche-Schmitz, G.S. Chhatwal, S.D. Bentley, J.D.

Fraser, N.J. Moreland, J.R. Carapetis, A.C. Steer, J. Parkhill, A. Saul, D.A. Williamson, B.J. Currie, S.Y.C. Tong, G. Dougan, M.J. Walker, Nat Genet, vol. 51, 2019, pp. 1035-1043.

[22] R.C. Edgar, Nucleic Acids Res, vol. 32, 2004, pp. 1792-1797.

[23] M. Kearse, R. Moir, A. Wilson, S. Stones-Havas, M. Cheung, S. Sturrock, S. Buxton, A. Cooper, S. Markowitz, C. Duran, T. Thierer, B. Ashton, P. Meintjes, A. Drummond, Bioinformatics, vol. 28, 2012, pp. 1647-1649.

[24] M.Y. Linova, M.W. Risor, S.E. Jorgensen, Z. Mansour, J. Kaya, J.J. Sigurdarson, J.J. Enghild, H. Karring, Protein Expr Purif, vol. 166, 2020, pp. 105507.

[25] E.B. Brazel, A. Tan, S.L. Neville, A.R. Iverson, S.R. Udagedara, B.A. Cunningham, M. Sikanyika, D.M.P. De Oliveira, B. Keller, L. Bohlmann, I.M. El-Deeb, K. Ganio, B.A. Eijkelkamp, A.G. McEwan, M. von Itzstein, M.J. Maher, M.J. Walker, J.W. Rosch, C.A. McDevitt, Cell Rep, vol. 38, 2022, pp. 110202.

[26] S.L. Neville, B.A. Eijkelkamp, A. Lothian, J.C. Paton, B.R. Roberts, J.W. Rosch, C.A. McDevitt, Commun Biol, vol. 3, 2020, pp. 694.

[27] T.M. McPhillips, S.E. McPhillips, H.J. Chiu, A.E. Cohen, A.M. Deacon, P.J. Ellis, E. Garman, A. Gonzalez, N.K. Sauter, R.P. Phizackerley, S.M. Soltis, P. Kuhn, J Synchrotron Radiat, vol. 9, 2002, pp. 401-406.

[28] W. Kabsch, Acta Crystallogr D Biol Crystallogr, vol. 66, 2010, pp. 125-132.

[29] P.R. Evans, G.N. Murshudov, Acta Crystallogr D Biol Crystallogr, vol. 69, 2013, pp. 1204-1214.

[30] P.D. Adams, P.V. Afonine, G. Bunkoczi, V.B. Chen, I.W. Davis, N. Echols, J.J. Headd, L.W. Hung, G.J. Kapral, R.W. Grosse-Kunstleve, A.J. McCoy, N.W. Moriarty, R. Oeffner, R.J. Read, D.C. Richardson, J.S. Richardson, T.C. Terwilliger, P.H. Zwart, Acta Crystallogr D Biol Crystallogr, vol. 66, 2010, pp. 213-221.

[31] J. Jumper, R. Evans, A. Pritzel, T. Green, M. Figurnov, O. Ronneberger, K. Tunyasuvunakool, R. Bates, A. Zidek, A. Potapenko, A. Bridgland, C. Meyer, S.A.A. Kohl, A.J. Ballard, A. Cowie, B.

Romera-Paredes, S. Nikolov, R. Jain, J. Adler, T. Back, S. Petersen, D. Reiman, E. Clancy, M. Zielinski, M. Steinegger, M. Pacholska, T. Berghammer, S. Bodenstein, D. Silver, O. Vinyals, A.W. Senior, K. Kavukcuoglu, P. Kohli, D. Hassabis, Nature, vol. 596, 2021, pp. 583-589.

[32] T.C. Terwilliger, R.W. Grosse-Kunstleve, P.V. Afonine, N.W. Moriarty, P.H. Zwart, L.W. Hung, R.J. Read, P.D. Adams, Acta Crystallogr D Biol Crystallogr, vol. 64, 2008, pp. 61-69.

[33] P.V. Afonine, R.W. Grosse-Kunstleve, N. Echols, J.J. Headd, N.W. Moriarty, M. Mustyakimov, T.C. Terwilliger, A. Urzhumtsev, P.H. Zwart, P.D. Adams, Acta Crystallogr D Biol Crystallogr, vol. 68, 2012, pp. 352-367.

[34] P. Emsley, B. Lohkamp, W.G. Scott, K. Cowtan, Acta Crystallogr D Biol Crystallogr, vol. 66, 2010, pp. 486-501.

[35] L. Schrödinger, W. DeLano, http://www.pymol.org/pymol, 2020.

[36] M.J. Abraham, T. Murtola, R. Schulz, S. Páll, J.C. Smith, B. Hess, E. Lindahl, SoftwareX, vol. 1-2, 2015, pp. 19-25.

[37] Lindahl., Abraham., Hess., V.d. Spoel., Zenodo, 2020.

[38] N. Schmid, A.P. Eichenberger, A. Choutko, S. Riniker, M. Winger, A.E. Mark, W.F. van Gunsteren, Eur Biophys J, vol. 40, 2011, pp. 843-856.

[39] P.J.P.M. Berendsen H.J.C, van Gunsteren W.F, Hermans J, Intermolecular Forces, vol. 14, 1981, pp. 331-342.

[40] N. Michaud-Agrawal, E.J. Denning, T.B. Woolf, O. Beckstein, J Comput Chem, vol. 32, 2011, pp. 2319-2327.

[41] W. Humphrey, A. Dalke, K. Schulten, J Mol Graph, vol. 14, 1996, pp. 33-38, 27-38.

[42] X. Daura, K. Gademann, B. Jaun, D. Seebach, W.F. van Gunsteren, A.E. Mark, Angew Chem Int Ed, vol. 38, 1999, pp. 236-240.

[43] L.A. Yatsunyk, J.A. Easton, L.R. Kim, S.A. Sugarbaker, B. Bennett, R.M. Breece, Vorontsov, II, D.L. Tierney, M.W. Crowder, A.C. Rosenzweig, J Biol Inorg Chem, vol. 13, 2008, pp. 271-288.

[44] D.C. Desrosiers, S.W. Bearden, I. Mier, Jr., J. Abney, J.T. Paulley, J.D. Fetherston, J.C. Salazar, J.D. Radolf, R.D. Perry, Infect Immun, vol. 78, 2010, pp. 5163-5177.

[45] S. Banerjee, B. Wei, M. Bhattacharyya-Pakrasi, H.B. Pakrasi, T.J. Smith, J Mol Biol, vol. 333, 2003, pp. 1061-1069.

[46] B. Wei, A.M. Randich, M. Bhattacharyya-Pakrasi, H.B. Pakrasi, T.J. Smith, Biochemistry, vol. 46, 2007, pp. 8734-8743.

[47] D.C. Desrosiers, Y.C. Sun, A.A. Zaidi, C.H. Eggers, D.L. Cox, J.D. Radolf, Mol Microbiol, vol. 65, 2007, pp. 137-152.

[48] D. Lu, B. Boyd, C.A. Lingwood, J Biol Chem, vol. 272, 1997, pp. 29033-29038.

[49] E. Loisel, L. Jacquamet, L. Serre, C. Bauvois, J.L. Ferrer, T. Vernet, A.M. Di Guilmi, C. Durmort, J Mol Biol, vol. 381, 2008, pp. 594-606.

[50] F.H. Niesen, H. Berglund, M. Vedadi, Nat Protoc, vol. 2, 2007, pp. nprot.2007.2321.

[51] V. Putignano, A. Rosato, L. Banci, C. Andreini, Nucleic Acids Res, vol. 46, 2018, pp. D459-D464.

[52] B. Zheng, Q. Zhang, J. Gao, H. Han, M. Li, J. Zhang, J. Qi, J. Yan, G.F. Gao, PLoS One, vol. 6, Public Library of Science, 2011, pp. e19510.

[53] A. Hecel, A. Kola, D. Valensin, H. Kozlowski, M. Rowinska-Zyrek, Inorg Chem, vol. 59, American Chemical Society, 2020, pp. 1947-1958.

[54] C.D. Radka, S.G. Aller, Acta Crystallogr F Struct Biol Commun, vol. 77, 2021, pp. 286-293.

[55] S.L. Neville, J. Sjohamn, J.A. Watts, H. MacDermott-Opeskin, S.J. Fairweather, K. Ganio, A. Carey Hulyer, A.P. McGrath, A.J. Hayes, T.R. Malcolm, M.R. Davies, N. Nomura, S. Iwata, M.L. O'Mara, M.J. Maher, C.A. McDevitt, Sci Adv, vol. 7, 2021.

[56] S. Siche, O. Neubauer, P. Hebbeln, T. Eitinger, Res Microbiol, vol. 161, 2010, pp. 824-829.

[57] F. Finkenwirth, M. Sippach, S.N. Pecina, M. Gade, J. Ruta, A. Ricke, E. Bondarenko, J.P. Klare, M. Zinke, S. Lange, A. Lange, H.J. Steinhoff, T. Eitinger, Biochim Biophys Acta Biomembr, vol. 1862, 2020, pp. 183114.

[58] A. Ilari, F. Alaleona, P. Petrarca, A. Battistoni, E. Chiancone, J Mol Biol, vol. 409, 2011, pp. 630-641.

[59] D.P. Neupane, D. Avalos, S. Fullam, H. Roychowdhury, E.T. Yukl, J Biol Chem, vol. 292, 2017, pp. 17496-17505.

[60] R.M. Couñago, M.P. Ween, S.L. Begg, M. Bajaj, J. Zuegg, M.L. O'Mara, M.A. Cooper, A.G. McEwan, J.C. Paton, B. Kobe, C.A. McDevitt, Nat Chem Biol, vol. 10, 2014, pp. 35-41.

[61] M. Handali, H. Roychowdhury, D.P. Neupane, E.T. Yukl, J Biol Chem, vol. 290, 2015, pp. 29984-29992.

[62] Y.M. Lee, C. Lim, J Mol Biol, vol. 379, 2008, pp. 545-553.

Table of Abbreviations

A. baumannii, *Acinteobacter baumannii*

ABC, ATP-binding cassette

Cα, alpha carbon

CDC, Centers for Disease Control and Prevention

DSF, differential scanning fluorimetry

ECF, energy-coupling factor

EDTA, ethylenediaminetetraacetic acid

E. coli, *Escherichia coli*

His, histidine

ICP-MS, inductively coupled plasma-mass spectrometry

IMAC, immobilized metal ion affinity chromatography

MD, molecular dynamics

MOPS, 3-(*N*-morpholino)propanesulfonic acid

MWCO, molecular weight cutoff

N-terminal, amino-terminal

P. denitrificans, *Paracoccus denitrificans*

RMSD, root mean square deviation

SBP, solute-binding protein

SDS-PAGE, sodium dodecyl sulfate–polyacrylamide gel electrophoresis

S.E.M., standard error of the mean

S. enterica, *Salmonella enterica*

S. pneumoniae, *Streptococcus pneumoniae*

TPEN, *N,N,N′,N′*-tetrakis(2-pyridinylmethyl)-1,2-ethanediamine

T_m, melting transition

WHO, World Health Organization

Figure 1

Click here to access/download;Figure;Figure 1 - Multiple Sequence Alignment_Final.tif

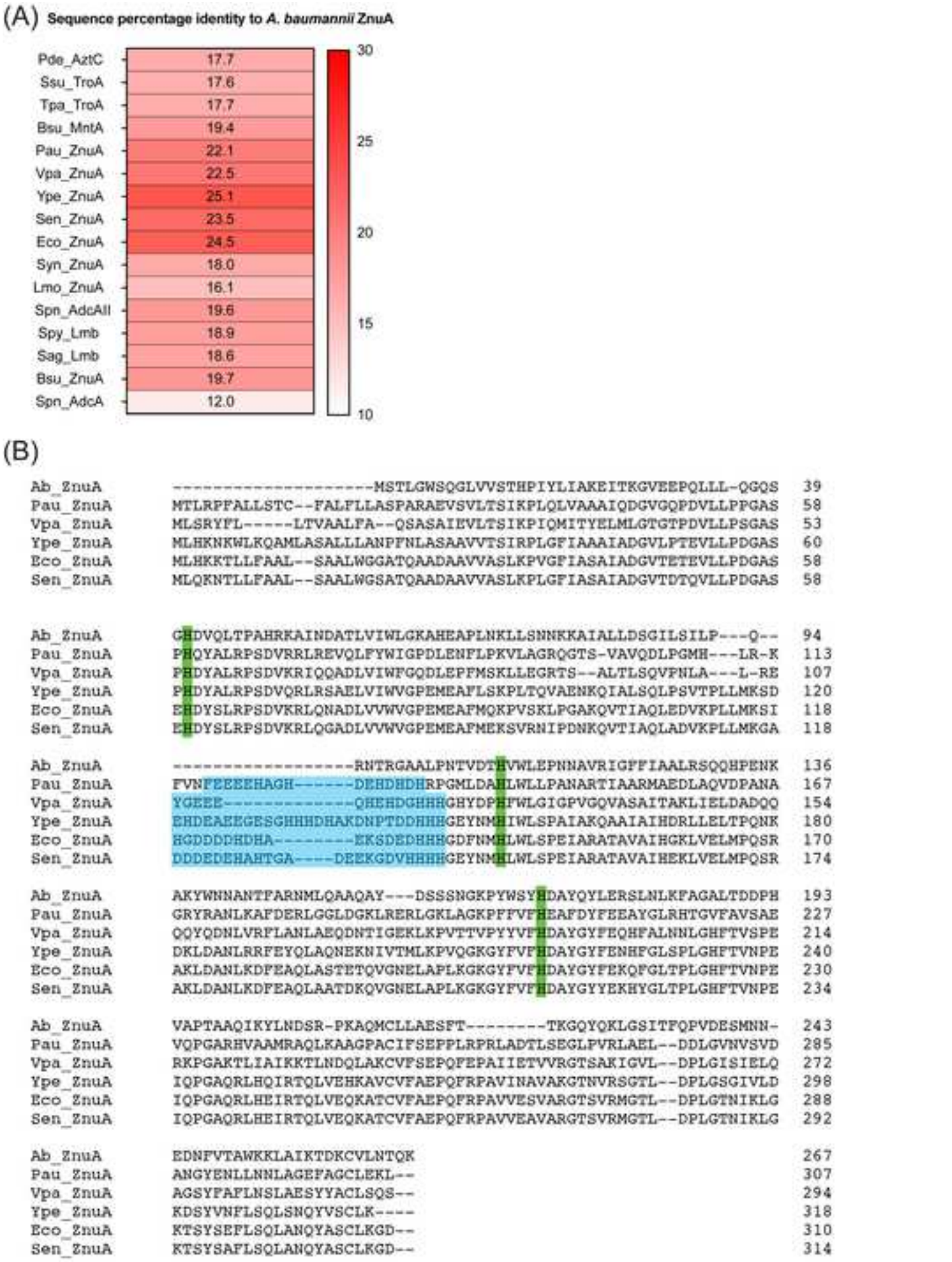


Figure 2

Click here to access/download;Figure;Figure 2 - Protein_Final.tif

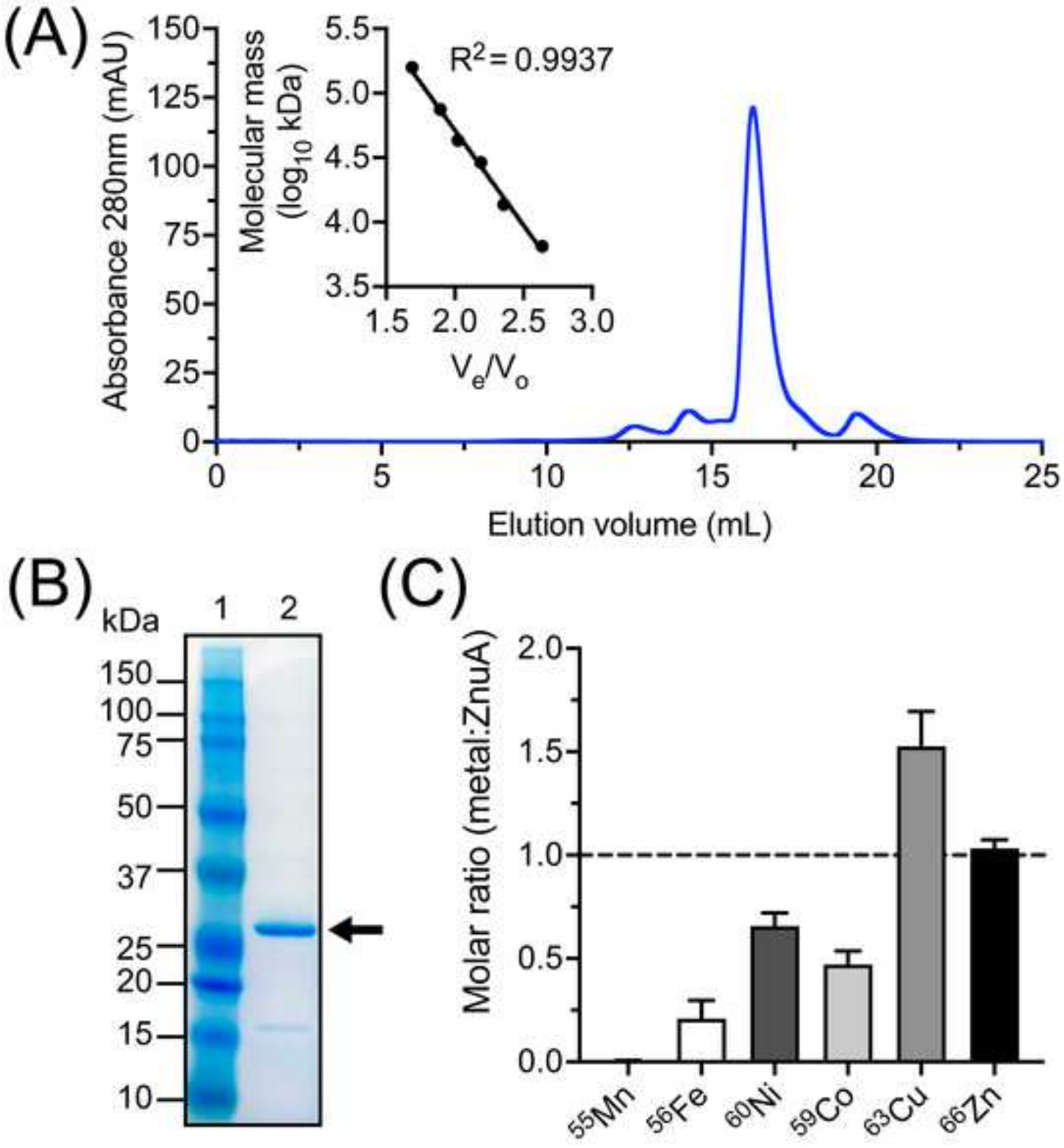


Figure 3

Click here to access/download;Figure;Figure 3 - Structure_Final.tif

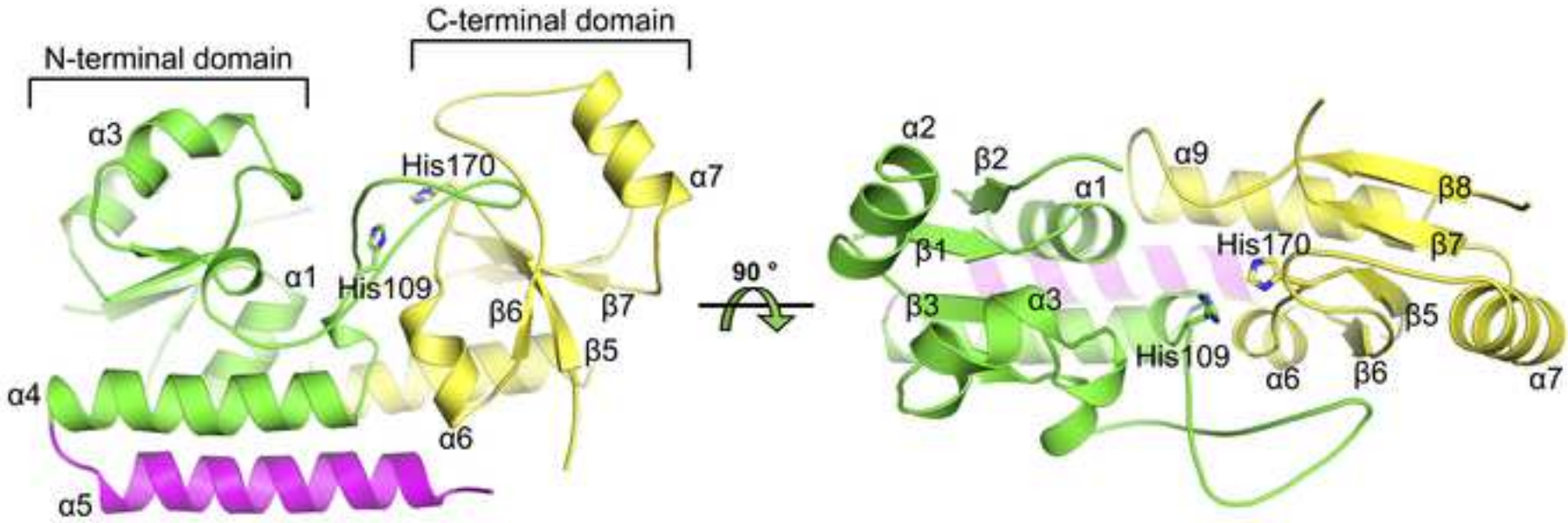


Figure 4

Click here to access/download;Figure;Figure 4_Final.tif

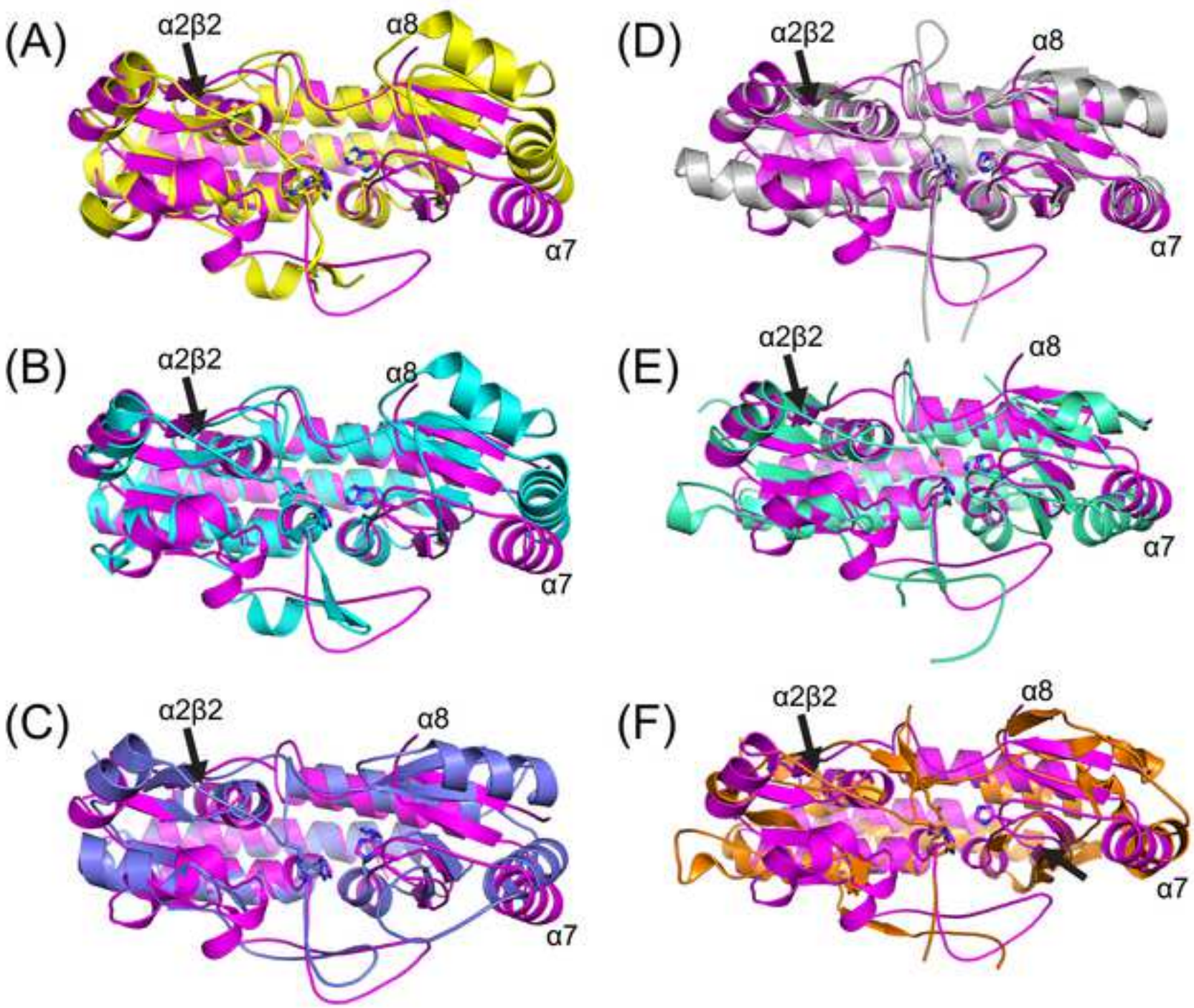


Figure 5

Click here to access/download;Figure;Figure 5 - MD_Final.tif

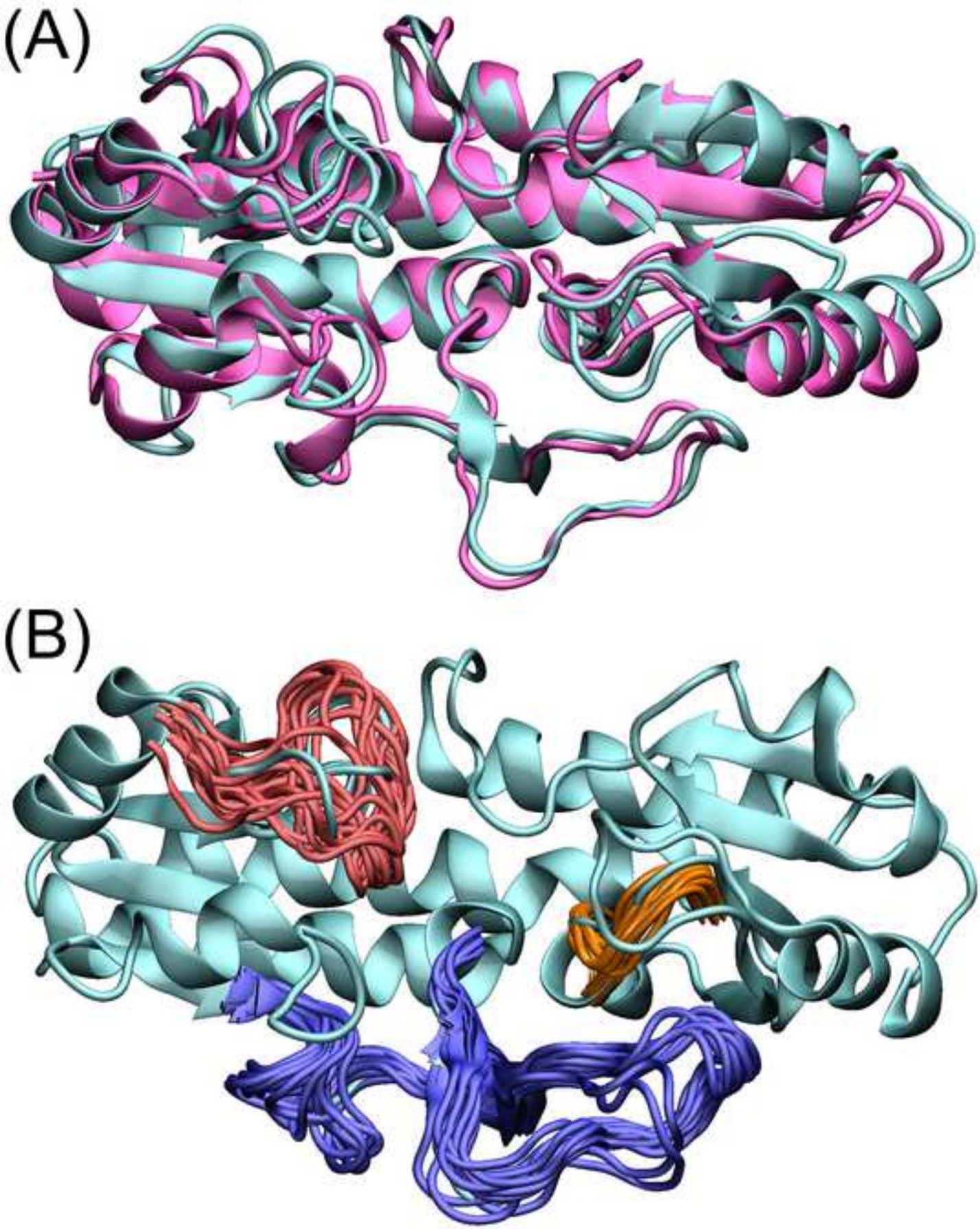
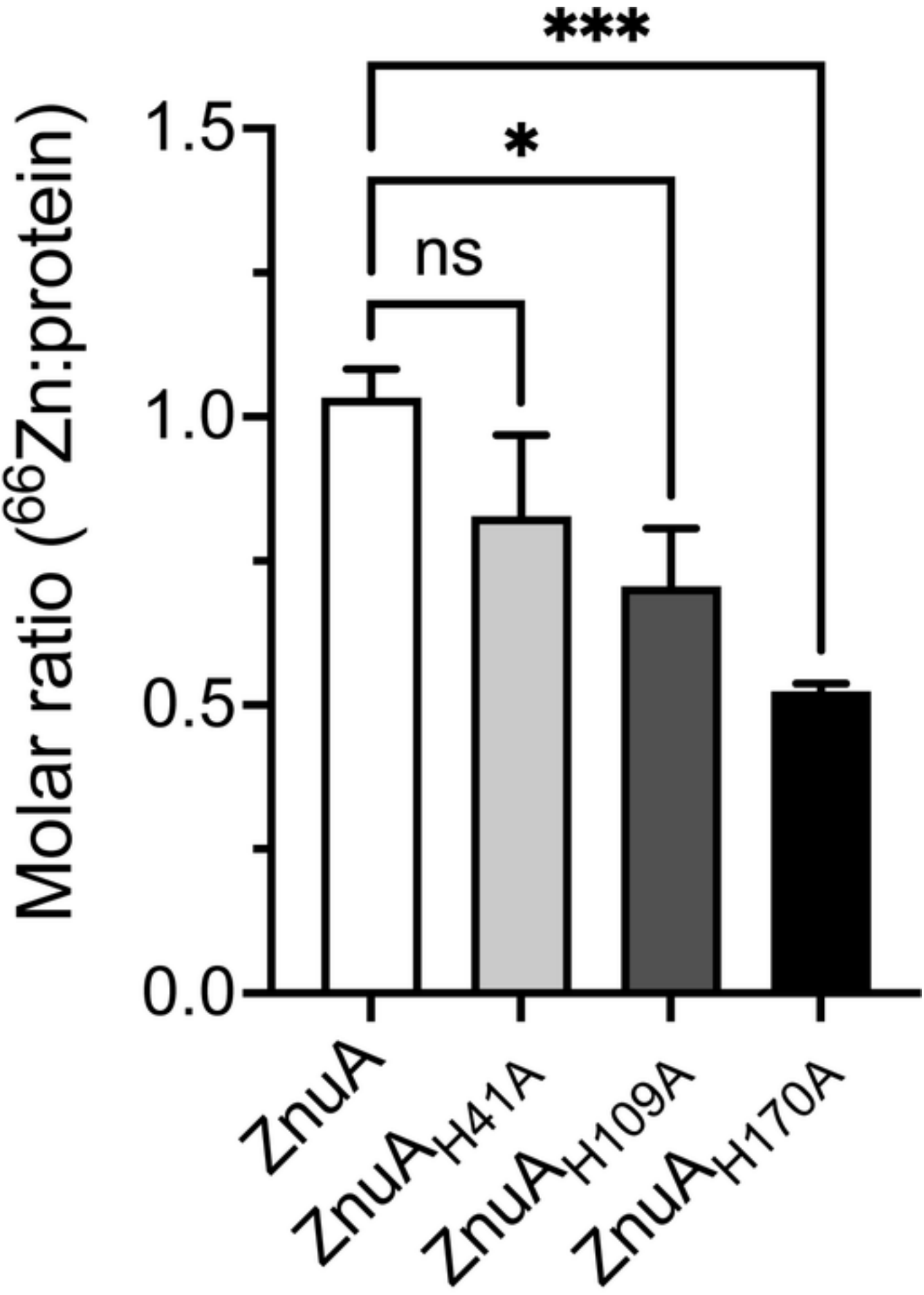


Figure 6

Click here to access/download;Figure;Figure 6 - Mutants_Final.tif



Declaration of interests

☐The authors declare that they have no known competing financial interests or personal relationships that could have appeared to influence the work reported in this paper.

☒The authors declare the following financial interests/personal relationships which may be considered as potential competing interests:

Christopher McDevitt reports financial support was provided by National Health and Medical Research Council. Christopher McDevitt reports financial support was provided by Australian Research Council. Bostjan Kobe reports financial support was provided by National Health and Medical Research Council. Bostjan Kobe reports financial support was provided by Australian Research Council.

Saleh Alquethamy: Investigation, Methodology, Data curation, Formal analysis, Writing-Original draft preparation.

Katherine Ganio: Investigation.

Zhenyao Luo: Investigation, Formal analysis, Visualization.

Sheik Imammul Hossain: Investigation, Formal analysis, Visualization.

Andrew J. Hayes: Investigation, Formal analysis.

Thomas Ve: Formal analysis.

Mark R. Davies: Formal analysis, Supervision.

Evelyne Deplazes: Investigation, Formal analysis, Funding acquisition, Writing - Review & Editing.

Boštjan Kobe: Writing - Review & Editing, Supervision, Funding acquisition.

Christopher A. McDevitt: Conceptualization, Methodology, Resources, Formal analysis, Writing - Original Draft, Writing - Review & Editing, Supervision, Project administration, Funding acquisition.

Click here to access/download
Supplementary Material
Alquethamy_Supplementary_Final.pdf

Supplementary Table 3



Click here to access/download

Supplementary Material

Table S3.xlsx